RSC Advances

ROYAL SOCIETY OF CHEMISTRY

www.rsc.org/advances

Journal Name

ARTICLE

Monodisperse FePt nanoparticles as highly active electrocatalysts for methanol oxidation

Received 00th January 20xx,
Accepted 00th January 20xx

DOI: 10.1039/x0xx00000x

www.rsc.org/

Shuai Liang,[a] Fei Wang,[a] Zhenwei Zhang,[b] Yaqing Li,[a] Yunliang Cai,[a] Jing Ren,[a] Xingmao Jiang[a,*]

Face-centered tetragonal (fct) FePt nanoparticles were successfully synthesized by a new and facile approach based on reverse microemulsion method. TEM results exhibited that highly dispersed FePt nanoparticles with size of about 3 nm and narrow size distribution can be achieved by this process. These fct FePt nanoparticles exhibited greatly enhanced catalytic activity towards the electro-oxidation of methanol compared with either Pt-based (Co, Ni) or Pt catalysts prepared by the same method owing to the unique core/shell structure and properties of Fe atoms. FePt nanoparticles wrapped in NaCl formed core-shell structure, which prevent nanoparticles form sintering and growth under high temperature calcination and ensured high monodispersity and size uniformity of FePt nanoparticles. The synthesis provides an indication for future development of multicomponent nanoparticles for advanced catalytic applications.

1.Introduction

In recent decades, fuel cells have drawn great attention as alternative energy sources due to the depletion of fossil fuels and the increase in environmental pollution.[1] As one types of fuel cells, the direct methanol fuel cell (DMFC) is a superior power source for applications in transportation[2] and portable electronic devices[3] because of its low operating temperature,[4] high energy density,[5] low pollutant emission[6] and simplicity of handling and processing of liquid fuel.[7] However, fully reflecting the DMFC performance mainly depends on the activity and durability of its electrocatalyst.[4, 7, 8] At present, platinum (Pt) nanoparticles has been demonstrated as the most efficient catalyst for low-temperature fuel cells among different types of electrocatalysts.[9, 10] Unfortunately, high cost and finite availability do not allow Pt to be used at a commercial level. To overcome these obstacles, how to design and synthesize more efficient Pt-based electrocatalysts for cost-effective and availability fuel cell devices attracts wide spread interest from researchers.

Up to now, many study focus on decreasing the Pt content in fuel cell catalysts through the effective strategy of alloying Pt with other inexpensive metals, such as Fe, Co, Ni, Cu, Zn, Cd, Hg, Pb and Sn.[11-19] Recently, lots of works have been reported on FePt alloys due to their $L1_0$ phase with large uniaxial magnetocrystalline anisotropy [$Ku \approx 6.6\times10^7$ J m^{-3}][20-22] and good chemical stability.[23] In addition, FePt alloys can be served as a more practical catalyst for oxygen reduction reaction (ORR) in fuel cells.[21] For example, Sun et al.[24] have prepared structurally ordered FePt nanoparticles which enhanced catalytic performance for oxygen reduction reaction. However, a chemically ordered face-centered tetragonal (fct) structure FePt must be prepared under high temperature condition, which leads to aggregation or sintering of nanoparticles[25]. Hence, how to synthesize high-quality monodisperse FePt nanoalloy as high-performance electrocatalysts through a simple approach becomes an interesting topic and challenging problem.

In this work, we developed a new and simple approach based on reverse microemulsion method that produced monodisperse FePt nanoparticles with controlled size and composition. Moreover, we also have obtained FePt/NaCl core/shell nanoparticles through azeotropic distillation by removing the water solution after a certain time of inverse microemulsion. In this way, monodisperse FePt nanoparticles were obtained and exhibited high electrocatalytic activity for methanol oxidation. These FePt nanoparticles are a promising catalyst for practical fuel cell applications. The main text of the article should appear here with headings as appropriate.

2.Experimental Section

2.1 Chemicals and Instrumentation

Hexadecyl trimethyl ammonium Bromide (CTAB, 99 %, Shanghai Aladdin industrial Co., Ltd.), (Hydro) chloroplatinic acid ($H_2PtCl_6\cdot6H_2O$, Pt 37.5 %, Shanghai Aladdin industrial Co., Ltd.), Iron(III) nitrate nonahydrate ($Fe(NO_3)_3\cdot9H_2O$, 99 %, Shanghai Aladdin industrial Co., Ltd.), Cobalt(II) nitrate

[a] Key Laboratory of Fine Petrochemical Engineering, Jiangsu Key Laboratory of Advanced Catalytic Materials and Technology, Changzhou University, Changzhou 213164, PR China.
[b] State Key Laboratory of Materials-Oriented Chemical Engineering, College of Chemistry and Chemical Engineering, Nanjing University of Technology, Nanjing 210009, PR China.
*Corresponding author: E-mail: jxm@cczu.edu.cn; Fax: +86 519 8633 0251; Tel: +86 519 8633 0253
Electronic Supplementary Information (ESI) available: [details of any supplementary information available should be included here]. See DOI: 10.1039/x0xx00000x

hexahydrate ($Co(NO_3)_2 \cdot 6H_2O$, 99 %, Shanghai Aladdin industrial Co., Ltd.), Nickel(II) nitrate hexahydrate ($Ni(NO_3)_2 \cdot 6H_2O$, 99 %, Shanghai Aladdin industrial Co., Ltd.), Sodium chloride (NaCl, 99 %, Shanghai Aladdin industrial Co., Ltd.), Benzene (C_6H_6, 99 %, Shanghai Aladdin industrial Co., Ltd.), Methyl alcohol (CH_3OH, 99.5%, Shanghai Aladdin industrial Co., Ltd.), Sulfuric acid (H_2SO_4, 98 %, Sinopharm Chemical Reagent Co., Ltd.).

The morphology and structures were determined by transmission electron microscopy (TEM, JEM-2100, JEOL) and powder x-ray diffraction (XRD, D/max 2500PC, Rigaku) with Cu Kα radiation. The electrochemical experiments were performed on a CHI 660D electrochemical workstation (Huake 101 Putian Instrumental Co., Beijing, China), use three electrodes system, reference electrode is saturated calomel electrode (SCE), the counter electrod is platinum electrod and glassy carbon electrode as working electrode (GCE). The cyclic voltammetry (CV) tests of methanol electrooxidation were carried out within a potential scope from -0.25 to 1.2 V in 0.5 M H_2SO_4 containing 0.5 M methanol at a scan rate of 100 mV s^{-1}.

2.2 Synthesis of fct-FePt nanoparticles

The preparing process can be described as follows. Firstly, 5 ml absolute aqueous solution containing the same mole of $H_2PtCl_6 \cdot 6H_2O$ (5×10^{-4} M), $Fe(NO_3)_3 \cdot 9H_2O$, 0.15 g NaCl and 5 ml deionized water was mixed by ultrasonic and 1.0 g CTAB (Hexadecyl trimethyl ammonium Bromide, $C_{19}H_{42}NBr$) and 100 ml Benzene (C_6H_6) were added to a three-neck flask. Secondly, the reaction system was stirred at 70 °C for 6 h and then the temperature increased to 90 °C to remove the water slowly through azeotropic distillation. Thirdly, the dried sample was calcined at 500 °C for 5 h under the air, and then calcined at 700 °C for 4 h with 7 % H_2/Ar. Finally, the salts were removed from the samples by washing several times using deionized water and the solid products were obtained by centrifugation. Subsequently, a 10 μL dispersion of as-prepared FePt (2 mg mL^{-1}) was dropped on a GCE that was then allowed to dry in air. Afterwards, a 5 μL 5 % nafion (v/v) was dropped onto the electrode to help prevent leakage of solid during the testing process.

The preparation method of CoPt, NiPt and Pt nanoparticles was the same as fct-FePt nanoparticles.

2.3 Performance test

Because Pt catalysts can catalyse the redox reaction in H_2SO_4/0.5 M CH_3OH system, we here keep on studying the electrocatalytic activity of FePt nanoparticles modified glassy carbon electrode by cyclic voltammogram (CV) method in 0.5M H_2SO_4/0.5M CH_3OH solution. CV experiments were carried out in a conventional three-compartment electrochemical analyzer, in which a saturated calomel electrode (SCE) was used for the reference electrode and a platinum wire was used for the counter electrode.

Prior to modification, the bare glassy carbon electrode (GCE, 3 mm diameter) was polished with emery paper, then on leather. Subsequently, a mixture containing 6 mg FePt nanoparticles and 3 ml deionized water were ultrasonically blended in a glass vessel for half an hour to get well dispersed solution. Ten microliters of dispersed solution was spread on the surface of polished GCE by a conventional method-micropipetter and dried in room temperature for almost 30 min to obtain a thin active catalytic layer. Afterwards, a 5 μL 5 % nafion (v/v) was dropped onto the electrode to help prevent leakage of solid during the testing process. The electrolyte solution is 0.5 M H_2SO_4/0.5 M CH_3OH, CV was obtained from -0.25–1.2 V (SCE) at 100 mV s^{-1} scan rate. All the CV tests were carried out at room temperature.

3.Result and discussions

Fig. 1 showed the XRD patterns of the obtained FePt/NaCl after annealed for 4 h at 700 °C under 7 % H_2/Ar. It can be seen clearly that all diffraction peaks of the products that were not washed can be observed for NaCl crystal (JCPDS 5-0628)[26], which are indexed with (111), (200), (220), (311) at 2 θ values of 27.334 °, 31.692 °, 45.449 °, 53.852 °, respectively. And we found that no FePt peaks appeared in the Fig. 1a, which may be because FePt nanoparticles embedded in NaCl crystal, which greatly weakened their diffraction intensity. And after washing NaCl, as shown in Fig. 1, XRD patterns of the typical diffraction peaks for the ordered face centred tetragonal (fct) FePt (JCPDS 43-1359)[27] at 2 θ values of 23.966 °, 32.839 °, 41.049 °, 47.123 °, 49.041 ° for planes (001), (110), (111), (200), (002) appeared in the sample calcined at 700 °C for 4 h. Diffraction peaks related to NaCl or any other phases were not found, thus confirming the presence of only single-phase FePt alloy after washing several times using deionized water.

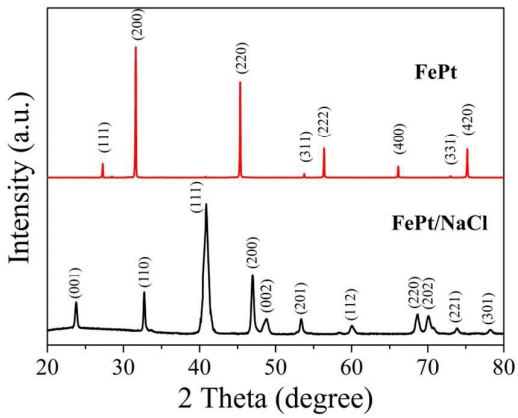

Fig. 1 XRD patterns of as-prepared FePt/NaCl and FePt samples.

Fig. 2a showed TEM image of obtained FePt nanoparticles calcined at 700 °C for 4 h. FePt nanoparticles were spherical and had uniform size. Size distribution was narrow and the particle diameter of the obtained FePt nanoparticles ranged between 2.1 nm and 3.9 nm (Fig. 2b), with average particle size at 3.0 nm on the assumption of Gaussian distribution. Fig. 2c showed that each nanoparticles are single crystals with a lattice spacing of about 0.22 nm, characteristic of the (111) planes in

the chemically ordered fct which was in good agreement with the XRD results.

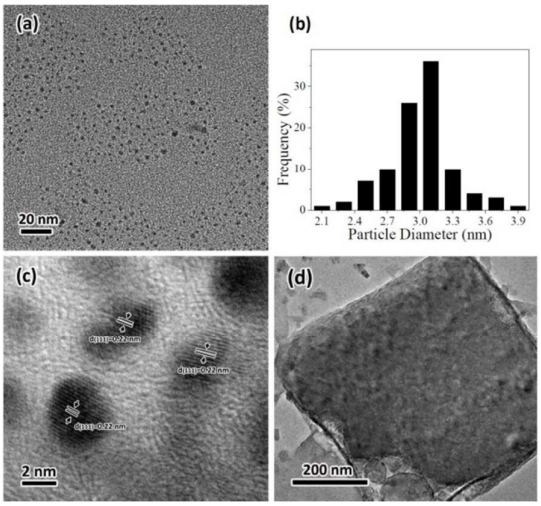

Fig. 2 TEM image (a), Particle size distribution (b), HRTEM image (c) of FePt sample and (d) TEM image of FePt/NaCl sample.

Fig. 2d suggested that because FePt nanoparticles wapped by NaCl crystal made the nanoparticles embedded in the NaCl crystal, which prevented the nanoparticles from contacting with each other during the high temperature calcination. Meanwhile, with the continuous electron beam irradiation, the FePt nanoparticles inside the NaCl crystal were gradually exposed.

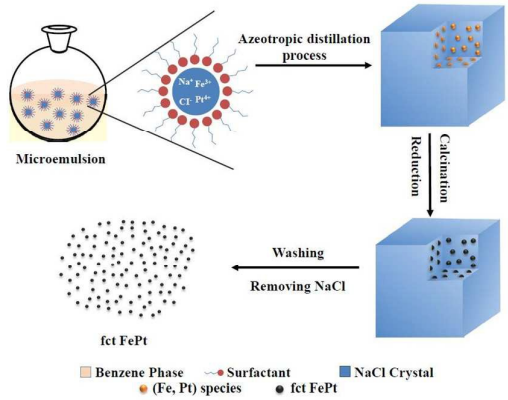

Scheme 1 Schematic illustration of the azeotropic distillation assisted route for the formation of the fct FePt nanoparticles.

On the basis of the above experimental results and analysis, a possible mechanism for fabrication of FePt nanoparticles was elucidated schematically in Scheme 1. Firstly, magnetic stirring of the heterogeneous solution in the presence of a surfactant generated a reverse microemulsion (water in oil). It is known that due to the interfacial phenomenon, the plurality of NaCl and metal salt aqueous solution droplets tend to disperse mono-sized and uniformly in a benzene phase. [28] During the process of the reverse microemulsion, surfactant micelles played an important role in controlling the process of crystal growth and stability of the particles. Then in the distillation process of reverse microemulsion, water could be gradually removed from the droplets in the form of a water–benzene azeotrope and cubic NaCl crystals could be formed within the interfacial film after a process of NaCl concentration, saturation, and crystallization. Meanwhile, (Fe, Pt) species that uniformly dispersed in the solvent embedded in the NaCl crystals during the crystallization of NaCl aggregation process. Depending on the cubic solid structure of NaCl crystals made the nanoparticles not contact each other, thus the uniform-sized and non-aggregation FePt nanoparticles could be finally obtained after the high-temperature calcination. The relatively slow evaporation process provided Na^+ and Cl^- ions by enough time for diffusion and crystallization[29] and made all the nanoparticles as far as possible embedded in the NaCl crystals. Then the samples were calcined at 500 °C for 5 h in air to remove the surfactant and followed by calcination at 700 °C for 4 h under 7 % H_2/Ar. As a result, the samples owning the structure of FePt/NaCl core-shell can be obtained. Finally, we obtained uniform and monodisperse FePt nanoparticles by washing to remove NaCl.

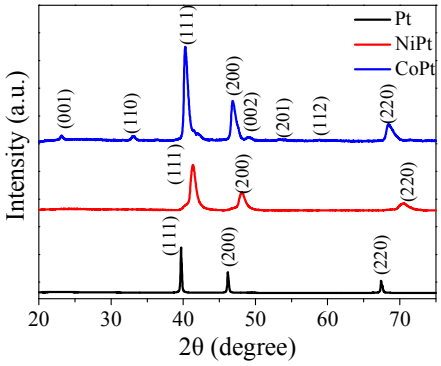

Fig. 3 XRD patterns of CoPt, NiPt and Pt nanoparticles.

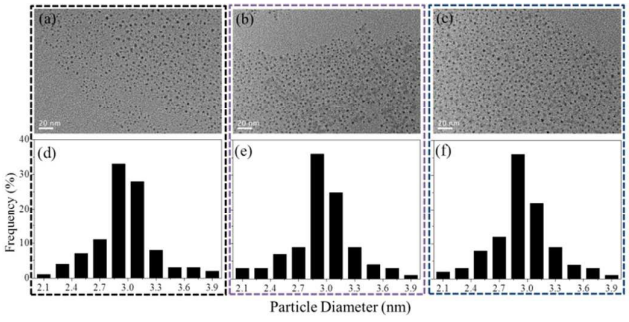

Fig. 4 TEM images and particle size distributions of CoPt (a, d), NiPt (b, e) and Pt nanoparticles (c, f).

In order to evaluate the electrocatalytic activities of FePt, CoPt, NiPt and Pt nanoparticles were chosen for comparison with the FePt nanoparticles, which were prepared by the same method that referred in the experimental section. As shown in Fig. 3, CoPt (JCPDS 43-1358)[30], NiPt (JCPDS 65-2797)[31] and Pt (JCPDS 04-0802)[32] nanoparticles were successfully obtained via this same way. Fig. 4(a-c) showed that all as-synthesized CoPt, NiPt and Pt nanoparticles had good dispersion and uniform particle size. In addition, the size distribution of CoPt, NiPt and Pt nanoparticles was shown in Fig. 4(d-f), respectively. Particle size of all samples ranged

between 2.1 nm and 3.9 nm, with average particle size at 3.0 nm on the assumption of Gaussian distribution as same as FePt nanoparticles.

The electrochemical performance of the FePt, CoPt, NiPt and Pt nanoparticles was investigated using cyclic voltammograms (CV) at a scan rate of 100 mV s^{-1} in 0.5 M H_2SO_4 solution. For comparison the CV results of these Pt-containing electrocatalysts were shown in Fig. 5. The current densities were normalized according to the electrochemically active surface areas (ECSAs), which was calculated from the corresponding charge of the hydrogen adsorption peak divided by the formation charge of a hydrogen adsorption monolayer deposited on polycrystalline platinum surface (210 μC cm^{-2}).[33]

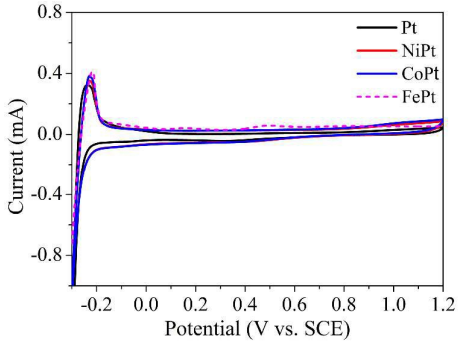

Fig. 5 Cyclic voltammograms of the samples in 0.5 M H_2SO_4 solution. Scan rate: 100 mV s^{-1}.

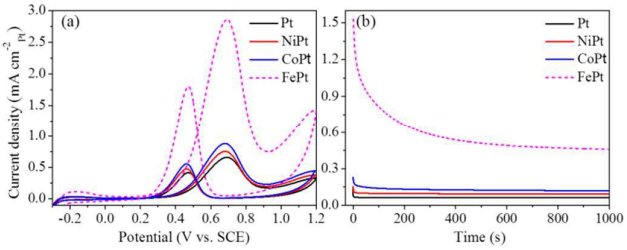

Fig. 6 Cyclic voltammograms of methanol oxidation on different catalysts in 0.5 M H_2SO_4 + 0.5 M CH_3OH solution at room temperature, with a scan rate of 100 mV s^{-1} (a). The current was normalized to the electrochemical surface areas of these catalysts. Chronoamperometry of methanol oxidation on different catalysts in 0.5 M H_2SO_4 + 0.5 M CH_3OH, potential controlled at 0.7 V (b).

The CVs of the FePt, CoPt, NiPt and Pt nanoparticles in 0.5 mol L^{-1} H_2SO_4 + 0.5 mol L^{-1} CH_3OH were shown in Fig. 6. The methanol oxidation current density was normalized by the platinum surface area, measured by the hydrogen adsorption desorption observed between +0.01 and -0.25 V. (vs. saturated calomel electrode (SCE)) in the CV curves (Fig. 6a). The FePt nanoparticles catalysts clearly showed higher specific activity for methanol oxidation at 0.5 V vs. SCE (forward peak current density) than the other Pt-based and Pt catalyst. For example, the peak current densities of methanol oxidation in the forward (positive) potential scan were 2.85, 0.89, 0.75 and 0.65 mA cm^{-2} for FePt, CoPt, NiPt and Pt nanoparticles catalysts, respectively. The activity of the obtained FePt nanoparticles for 4 h was 4.4 times greater than that of Pt catalysts. Chronoamperometry (CA) was conducted at 0.5 V vs. SCE to evaluate the current density change as a function of time. The current-time response at 0.5 V for 1000 s was shown in Fig. 6b. In according with the CV results, the methanol oxidation current densities of FePt nanoparticles catalysts were higher than those of Pt-based and Pt catalysts at 0.5 V over the entire time period examined. The current densities of the FePt nanoparticles decayed more slowly than the Pt-based and Pt catalysts. To the end of the 1000 s, the methanol oxidation current density of the FePt nanoparticles catalysts (0.47 mA cm^{-2}) was about 6 times that of Pt catalysts (0.08 mA cm^{-2}), which indicated that FePt had higher catalytic stability. Combined with cyclic voltammetry measurements above, this result further confirmed the superior catalytic activity and stability of FePt nanoparticles catalyst toward methanol oxidation. This was because that a Pt skin was formed during the repetitive potential cycling due to the dissolution of Fe on the alloy surface. The strong modification in the electronic structure of the Pt skin by the underlying Fe lowered the Fermi level at the alloy surface. The skin exhibited less electronic density in the d band.[34] The lowered electron density of the d orbital of Pt weakened the electron back-donation from Pt to CO, and consequently suppresses Pt–CO bonding, resulting in lowered CO coverage.[34-36] Thus, in the presence of Fe, there were more active sites than pure Pt or other Pt-based (Co, Ni) metals for methanol oxidation.

4.Conclusions

In summary, we have demonstrated a new and facile approach based on reverse microemulsion method for synthesis of monodisperse fct FePt nanoparticles. The use of NaCl was the key factor resulting formation of the obtained fct FePt nanoparticles with highly monodispersity and uniform-sized. Owing to the unique core/shell structure and properties of Fe atoms, FePt nanoparticles exhibited higher electrocatalytic activity than either the Pt-based (Co, Ni) or Pt catalysts prepared by the same method in methanol oxidation. This novel approach brings forward a broad idea to synthesize other functional materials, even generating new metastable intermetallic alloys and a new opportunity to research and apply other fields.

Acknowledgements

This work was financially supported by the National Natural Science Foundation of China under Grant [No. 21373034]; the Specially Hired Professorship-funding of Jiangsu province under Grant [No. SCZ1211400001]; Changzhou Science and Technology Bureau for Changzhou Key Laboratory of Respiratory Medical Engineering [Grant No. CM20133005]; the start-up funds from Changzhou University Jiangsu province; Jiangsu key laboratory of advanced catalytic material and technology; and Key laboratory of fine petrochemical

engineering and PAPD of Jiangsu Higher Education Institutions.

Notes and references

1 L. F. Dong, R. R. S. Gari, Z. Li, M. M. Craig and S. F. Hou, *Carbon*, 2010, **4**, 781.
2 R. Devanathan, N. Idupulapati and M. Dupuis, *J. Mater. Res.*, 2012, **27**, 1927.
3 F. Achmad, S. K. Kamarudin, W. R. W. Daud and E. H. Majlan, *Appl. Energy*, 2011, **88**, 1681.
4 Z. Ji, G. Zhu, X. Shen, H. Zhou, C. Wu and M. Wang, *New J. Chem.*, 2012, **3**, 1774.
5 M. Jafarian, M. G. Mahjani, H. Heli, F. Gobal, H. Khajehsharifi and M. H. Hamedi, *Electrochim. Acta*, 2003, **48**, 3423.
6 J. B. Wu, Z. G. Li, X. H. Huang and Y. Lin, *J. Power Sources*, 2013, **224**, 1.
7 Y. Zhao, L. Fan, H. Zhong, Y. Li and S. Yang, *Adv. Funct. Mater.*, 2007, **17**, 1537.
8 J. H. Chen, M. Y. Wang, B. Liu, Z. Fan, K. Z. Cui and Y. F. Kuang, *J. Phys. Chem. B*, 2006, **110**, 11775.
9 J. B. Wu and H. Yang, *Acc. Chem. Res.*, 2013, **46**, 1848.
10 X. W. Zhou, Y. Gan, J. J. Du, D. N. Tian, R. H. Zhang, C. Y. Yang and Z. X. Dai, *J. Power Sources*, 2013, **232**, 310.
11 J. X. Guo, Y. F. Sun, X. Zhang, L. Tang and H. T. Liu, *J. Alloys Compd.*, 2014, **604**, 286.
12 J. F. Shen, Y. Z. Hu, C. Li, C. Qin and M. X. Ye, *Electrochim. Acta*, 2008, **53**, 7276.
13 X. Y. Geng, H. M. Zhang, W. Ye, Y. W. Ma and H. X. Zhong, *J. Power Sources*, 2008, **185**, 627.
14 Y. J. Liu, Y. Q. Huang, Y. Xie, Z. H. Yang, H. L. Huang and Q. Y. Zhou, *Chem. Eng. J.*, 2012, **197**, 80.
15 A. Sode, W. Li, Y. G. Yang, P. C. Wong, E. Gyenge, K. A. Mitchell and D. Bizzotto, *J. Phys. Chem. B*, 2006, **110**, 8715.
16 T. Ghosh, Q. Zhou, J. M. Gregoire, R. B. van Dover and F. J. DiSalvo, *J. Phys. Chem. C*, 2010, **114**, 12545.
17 Y. J. Kang, L. Qi, M. Li, R. E. Diaz, D. Su, R. R. Adzic, E. Stach, J. Li and C. B. Murray, *ACS nano*, 2012, **6**, 2818.
18 E. Antolini and E. R. Gonzalez, *Catal. Today*, 2011, **160**, 28.
19 Y. Liu, D. G. Li, S. H. Sun, *J. Mater. Chem.*, 2011, **21**, 12579.
20 S. H. Sun, *Adv. Mater.*, 2006, **18**, 393.
21 S. Chen, D. A. MacLaren, R. T. Baker, J. N. Chapman, S. Lee, D. J. Cole-Hamilton, P. André, *J. Mater. Chem.*, 2011, **21**, 3646.
22 S. S. Kang, Z. Y. Jia, S. F. Shi, D. E. Nikles and J. W. Harrell, *Appl. Phys. Lett.*, 2005, **86**, 062503.
23 S. H. Sun, C. B Murray, D. Weller, L. Folks and A. Moser, *Science*, 2000, **287**, 1989.
24 J. Kim, Y. Lee and S. H. Sun, *J. Am. Chem. Soc.*, 2010, **132**, 4996.
25 C. N. He, N. Q. Zhao, *J. Mater. Chem.*, 2012, **22**, 1297.
26 A. M. Chockla, B. A. Korgel, *J. Mater. Chem.*, 2009, **19**, 999.
27 R. F. C. Farrow, D. Weller, R. F. Marks, M. F. Toney, A. Cebollada and G. R. Harp, *J. Appl. Phys.*, 1996, **79**, 5968.
28 R. C. Tolman, *J. Chem. Phys.*, 1949, **17**, 333.
29 X. Jiang and C. J. Brinker, *J. Am. Chem. Soc.*, 2006, **128**, 4512.
30 O. Song-II, J. M. Yan, H. L. Wang, Z. L. Wang, Q. Jiang, *Int. J. Hydrogen Energy*, 2014, **39**, 3757.
31 J. Lai, L. Zhang, W. Qi, J. Zhao, M. Xu, W. Gao and G. Xu, *ChemCatChem*, 2014, **6**, 2255.
32 X. Wang, J. Zhuang, Q. Peng and Y. Li, *Nature*, 2005, **437**, 123.
33 J. J. W, J. H. Zhu, M. G. Zhou, Y. L. Hou and S. Gao, *CrystEngComm.*, 2012, **14**, 7574.
34 M. Watanabe, Y. M. Zhu and H. Uchida, *J. Phys. Chem. B*, 2000, **104**, 1766.
35 J. B. Xu, K. F. Hua, G. Z. Sun, C. Wang, X. Y. Lv and Y. J. Wang, *Electrochem. Commun.*, 2006, **8**, 985.
36 T. Toda, H. Igarashi, H. Uchida and M. Watanabe, *J. Electrochem. Soc.*, 1999, **146**, 3754.